Carotid Artery Pressure Estimation

Elizabeth Healey
HST
ehealey@mit.edu

Holly Jackson
EECS
hjackson@mit.edu

Alex Jaffe
EECS
jaffea@mit.edu

***Abstract*—We build a numerical model for determining lumen pressure for the right carotid artery in a human volunteer. We utilize force-coupled ultrasound (FCU) to acquire an ultrasound image stack showing a long-axis view of the artery coupled with force measurement. We develop a 1-D forward finite difference model to predict the displacements of tissue, carotid wall, and carotid lumen in response to a known force applied to the surface of the skin for each force-coupled ultrasound image. We nest this forward model into an iterative inverse model where we optimize the surrounding tissue and carotid wall stiffness and lumen pressure parameters to minimize the difference between predicted displacement and the FCU-observed displacement. In addition to average tissue and carotid wall stiffness parameters, we output carotid lumen pressure for each ultrasound image, giving us a sampled carotid lumen pressure wave. We validate the maximum and minimum (systolic and diastolic) pressure values with an oscillometric blood pressure cuff reading of the left brachial artery in the same human volunteer.**

I. Introduction & Motivations

Force-coupled Ultrasound (FCU) allows one to know the force vector applied by an ultrasound probe while simultaneously being able to observe deformations in the tissue due to that force vector [1]. Through observations made by FCU, one has the potential to derive clinically relevant internal properties of the body otherwise only possible to observe through invasive procedures [2]. Given we are able to create a physiologically accurate numerical model to describe the properties of the vessel of interest and the tissue surrounding it, we can utilize FCU to derive estimates for lumen pressure for a blood vessel able to be observed via ultrasound without bone in between the probe and the vessel [1] [2]. The ability to non-invasively and accurately estimate these clinical values should aid in diagnosis and monitoring of peripheral artery disease, atherosclerosis, hypertension, and hypotension for arteries as well as congestive heart failure and venous insufficiency for veins [2] [3]. The motivation for impacting cardiovascular disease in general is extremely high as it remains the top cause of death in the United States [4]. Validating measurements for most of these applications are confined to only invasive procedures [5] [6]. However, the brachial artery blood pressure cuff is able to provide a noninvasive validation measurement for systolic (peak) and diastolic (valley) lumen pressure for the brachial artery in addition to the diastolic pressure for the carotid artery [7] [8]. With this metric as a validation, we develop a nonlinear dynamic system describing a long-axis view of the right carotid artery allowing us to find carotid lumen pressure, carotid wall stiffness, and surrounding tissue stiffness given an FCU input by nesting a forward finite element model for displacement inside an iterative inverse model to determine the pressure and stiffness parameters.

II. Problem Formulation

Our problem is formulated using a finite difference approach where nodes represent discrete points along a 1-D axis in the ultrasound image. These points correspond to points in soft tissue, artery wall, and artery lumen. The model includes elasticity and viscosity parameters for each element in the system and includes the force from the FCU as an external source. The unknown states for the forward model are the displacements of the nodes as a result of the external force sources applied. The components of the system are discretized by nodes separated by Δx when the system is unperturbed. Similar to the Kelvin-Voigt model [9] [10], we assume linear stress-strain in all regions except for the anterior and posterior tissue, in which we assume a simplified quadratic version of a hyperelastic stress-strain relation [11]. The set the equations in our system that model the boundaries of component (tissue/wall/lumen) are listed below. The equations represent displacements at nodes in the following boundaries: posterior tissue and end of the frame (Eq.1), posterior tissue and posterior vessel wall (Eq.2), posterior vessel wall and lumen (Eq.3), lumen and anterior vessel wall (Eq.4), anterior vessel wall and anterior tissue (Eq.5), and anterior tissue and FCU probe (Eq.6).

$$\frac{dx_1}{dt} = \frac{1}{\eta_t}\Big[\frac{a_t}{\Delta x^2}(x_2 - x_1)^2 - \frac{a_t}{\Delta x^2}x_1^2\Big] \tag{1}$$

$$\frac{dx_N}{dt} = \frac{1}{\eta_t}\Big[\frac{\epsilon_w}{\Delta x}(x_{N+1} - x_N) - \frac{a_t}{\Delta x^2}(x_N - x_{N-1})^2\Big] \tag{2}$$

$$\frac{dx_M}{dt} = \frac{1}{\eta_w}\Big[\frac{p_l}{\Delta x}(x_{M+1} - x_M) - \frac{\epsilon_w}{\Delta x}(x_M - x_{M-1})\Big] \tag{3}$$

$$\frac{dx_K}{dt} = \frac{1}{\eta_l}\Big[\frac{\epsilon_w}{\Delta x}(x_{K+1} - x_K) - \frac{p_l}{\Delta x}(x_K - x_{K-1})\Big] \tag{4}$$

$$\frac{dx_{M'}}{dt} = \frac{1}{\eta_w}\Big[\frac{a_t}{\Delta x^2}(x_{M'+1} - x_{M'})^2 - \frac{\epsilon_w}{\Delta x}(x_{M'} - x_{M'-1})\Big] \tag{5}$$

$$\frac{dx_{N'}}{dt} = \frac{1}{\eta_t}\Big[u(t) - \frac{a_t}{\Delta x^2}(x_{N'} - x_{N'-1})^2\Big] \tag{6}$$

The nodes within each component are described by the equations below. Eq. 7 describes the lumen nodes, where i is in range (M, K). Eq. 8 describes the posterior and anterior vessel wall nodes, where i is in range (N, M) and (K, M'), respectively. Eq. 9 describes the posterior and anterior tissue nodes, where i is in range $(1, N)$ and (M', N'), respectively.

$$\frac{dx_i}{dt} = \frac{1}{\eta_l}\left[\frac{p_l}{\Delta x}(x_{i+1} - x_i) - \frac{p_l}{\Delta x}(x_i - x_{i-1})\right] \quad (7)$$

$$\frac{dx_i}{dt} = \frac{1}{\eta_w}\left[\frac{\epsilon_w}{\Delta x}(x_{i+1} - x_i) - \frac{\epsilon_w}{\Delta x}(x_i - x_{i-1})\right] \quad (8)$$

$$\frac{dx_i}{dt} = \frac{1}{\eta_t}\left[\frac{a_t}{\Delta x^2}(x_{i+1} - x_i)^2 - \frac{a_t}{\Delta x^2}(x_i - x_{i-1})^2\right] \quad (9)$$

In the above equations, $u(t)$ is the force transferred through the FCU, and the parameters are given by a_t as the nonlinear tissue stiffness parameter, ϵ_w as the vessel stiffness parameter, p_l as the lumen pressure parameter, and η_t, η_w, and η_l as the tissue, vessel wall, and lumen viscosity parameters, respectively. Figure 1 illustrates the set of equations representing our model with minimal component discretization.

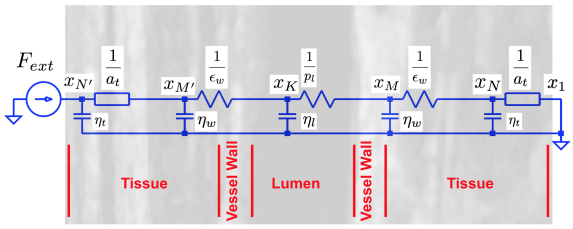

Fig. 1. Long-axis carotid image with system model and different constitutive layers overlaid in blue and red, respectively. The regions in the ultrasound image correspond to the labels in red. The circuit components in blue do not perfectly align with the layers.

We can combine these equations into a system of equations,

$$\frac{dx}{dt} = Ax + bu(t) = f(x, u)$$

$$y = cx(t)$$

where A is the Jacobian system matrix and b is the vectorization of the force input, $u(t)$. Matrix A is of dimension N' by N' and represented by a sparse matrix where there are no more than 3, and no less than 2, non-zero elements in any given row. The output of our system is represented by y and matrix c provides the transformation of the state to the output.

III. Fundamental Numerical Methods

The forward model of this system is solved by assuming steady state of tissue displacement. This assumption is made due to the fact that the time constant for the system given by the viscosity parameters, is significantly less than the sampling rate of the ultrasound given a slow ramp in force [12]. We solve the system $\frac{dx}{dt} = f(x, u) = 0$ using Newton's method for multidimensional systems [13]. This involves linearizing the system by analytically computing the Jacobian of $f(x, u)|_x$. We choose a convergence tolerance that is lower than the resolution of the ultrasound image. The forward solver is given in Alg. 1. In the implementation of our model, we use a total of 601 nodes. This corresponds to nodes placed 100 μm apart across a total distance of 6 cm. This creates a sparse matrix $J(x)$ and enables MATLAB to use LU decomposition to solve the system in the following pseudocode, saving overall computational time.

Algorithm 1 Forward Model Solver

set initial x_0 guess
set i to 0
while $\|f(x_k)\| >$ tolerance **or** $\|\Delta x\| >$ tolerance **do**
  Compute $f(x_k)$ and Jacobian, $J(x_k)$
  Solve $\Delta x = -J(x_i) \backslash f(x_i)$
  $x_{i+1} \leftarrow x_i + \Delta x$
  $i \leftarrow i + 1$
end
Result: Return Δx

IV. The Technical Challenge

Our technical challenge involves nesting the forward model to determine displacements of nodes in tissue, carotid artery wall, and carotid artery lumen into an iterative inverse model to determine the parameters of anterior tissue stiffness, carotid wall stiffness, and carotid lumen pressure for each ultrasound frame. For each ultrasound frame, we segment the image to track four important points at the boundaries between the anterior tissue and the anterior carotid wall, the anterior carotid wall and the carotid lumen, the carotid lumen and the posterior carotid wall, and the posterior carotid wall and the posterior tissue. Using this segmentation, we get the region size for anterior tissue, anterior carotid wall, lumen, and posterior carotid wall. For each ultrasound frame a vector, y_0, is generated with four entries describing how much each region displaced from an initial set starting point.

In applying force with the ultrasound probe as a function of time, we slowly ramp up the force and assume the system has achieved steady state in between each frame. In order to solve for the parameters at each frame given our forward model and our force and segmentation observations from our force-coupled ultrasound, we must solve an optimization problem minimizing the difference between the displacement observed and the displacement predicted by the model as a function of the parameters.

Algorithm 2 Iterative Inverse

for each ultrasound frame, i **do**
  get $y_{0,i}$ from ultrasound image, get force data, u_i
  while $g(x,p) = (y_{0,i} - cx_i(p))^T(y_0 - cx_i(p)) > tol$ **do**
    $x_{m,i} \leftarrow forwardmodel(p, u_i)$
    $p = p \odot cx_i \oslash y_{0,i}$
  end
  save $p_i = p$
end

Here, $g(x, p)$ is the cost function and is represented as a squaring scalar product of the difference between the node displacement of the model at the ith iteration $cx_{m,i}$ and the observed segmentation displacements y_0. Here, c represents a transformation from all node displacements x to the regional compression we can analogously observe in segmentation. We

select a convergence tolerance tol that is much less than the square of the ultrasound image resolution. We find the parameter estimate for the next iteration by multiplying the current parameters by the fraction of the predicted compression over the observed compression. We have elected this optimization strategy due to its relatively low computational complexity of $O(N'P)$ for each iteration outside of the forward model, where N' is the number of distinct nodes and P is the number of distinct parameters.

Once we run the iterative inverse optimization for each ultrasound frame in the selected force sweep, we wind up with the quadratic anterior tissue stiffness parameter a_t, the linear anterior and posterior carotid vessel wall stiffness parameters $\epsilon_{w,a}$ and $\epsilon_{w,p}$, and the carotid lumen pressure parameters p_l. We note that we allow for the parameters of anterior and posterior carotid vessel wall stiffness to be different, hence the two distinct subscript descriptors. Only p_l should vary significantly as a function of time. In the period of a cardiac cycle, a systolic pressure $\max(p_{l,T})$ and a diastolic pressure $\min(p_{l,T})$ where T symbolizes the frames within one cardiac cycle.

V. Results

A. Forward Model

Figure 2 shows the steady state displacements of 601 nodes distributed across tissue (blue), vessel wall (green), and lumen (red) under different external pressures predicted with our forward solver. The figure shows a set of 25 independent external pressures evenly spaced from 0 kPa to the lumen collapse force of 14 kPa. The nonlinear behavior of the tissue is visible in the figure. The tissue compresses quadratically with respect to applied pressure, while the other components have a linear relationship between predicted displacement and external pressure.

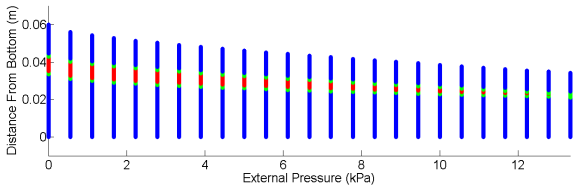

Fig. 2. Tissue (blue), vessel wall (green), and lumen (red) positions for a 601-node 1-D strip. Displacements predicted at increasing external pressures using forward finite difference model using estimated values for tissue, vessel wall, and lumen parameters.

B. Iterative Inverse Model

In order to obtain the observations necessary to run the iterative inverse model, we must obtain data with a force-coupled ultrasound device as seen in Figure 3 on the upper left. User-applied external force approximating a ramp is applied to track the displacements of the observed nodes over time as seen in Figure 3 upper on the right.

We must also segment ultrasound images taken with the force-coupled ultrasound in order to calculate the cost function

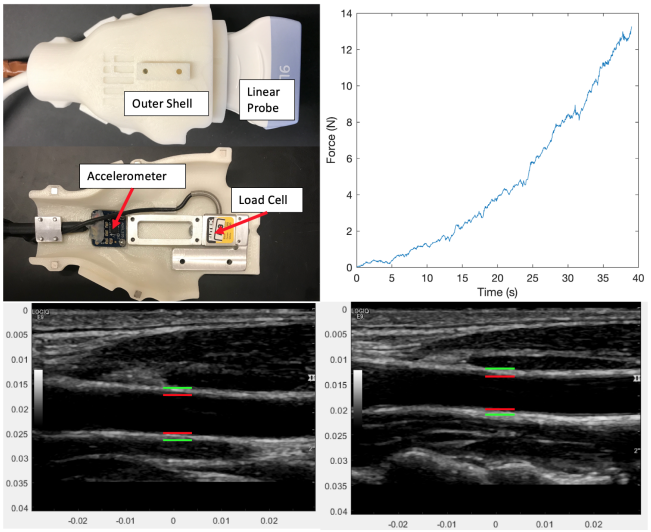

Fig. 3. Force-coupled ultrasound setup (top left) and force sensed during force ramp (top right). Long-axis view of carotid artery in systole and under low force (bottom right) ($\approx 0N$) and high force (bottom left) ($\approx 12N$) (bottom). The annotations signify the carotid lumen in between the red horizontal lines and the anterior and posterior carotid vessel walls in between a red horizontal line and a green horizontal line

for the iterative inverse model. We illustrate the segmentation in the bottom of Figure 3.

The iterative inverse model with the forward model embedded allows us to determine the parameters of our system through our observations from the force-coupled ultrasound, as previously mentioned. For each frame within the selected range of the force sweep, we run our optimization comparing our forward model output to our observations and arrive at converged values of our parameters. Table I shows the average (arithmetic mean) values along with the coefficient of variation (CV) obtained from running the iterative inverse model on the ultrasound frames within the selected force sweep range.

TABLE I
Carotid wall stiffness and surrounding tissue quadratic stiffness parameters mean and CV

Output	Mean	CV	Units
Anterior Wall Stiffness $\epsilon_{w,a}$	21.0	0.0065	kPa
Posterior Wall Stiffness $\epsilon_{w,p}$	7.99	0.058	kPa
Tissue Quadratic Stiffness a_t	124	0.10	kPa*m

TABLE II
Summary of carotid lumen pressure values with blood pressure cuff comparison.

Output	Mean	CV	Cuff	Units
Systolic $\max(p_{l,T})$	126.7	0.16	119	mmHg
Diastolic	61.5	0.046	75	mmHg
Mean	93.3	0.27	90	mmHg

We note that the values found for anterior carotid wall stiffness are in the ballpark of the values found for the brachial artery during a similar published study [14].

The carotid lumen pressure should vary as a function of time and has clinically relevant maximum and minimum values of systolic and diastolic pressures. The average and CV of the systolic and diastolic pressures over the selected range of the force sweep are displayed in Table II. The blood pressure cuff systolic and diastolic pressure is also displayed.

Using a 5-point moving average filter, the iterative inverse output carotid lumen pressure wave is shown in Figure 4. We see clearly the high CV for the systolic peaks and the low CV for the diastolic valleys.

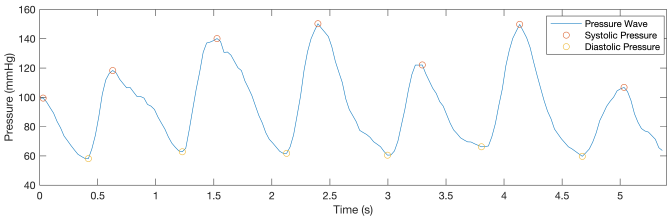

Fig. 4. Reconstructed carotid lumen pressure wave subject to a 5-point moving average filter during a 5.4 second window within force sweep ramping from 9.7 N to 12.5 N. Systolic peaks (red) and diastolic valleys (yellow) are shown.

Regarding runtime, there are 180 ultrasound frames for which to find our parameters over a 5.4 second time window. The code takes about 28 seconds in total to run for this time window. Therefore, each frame takes about 0.16 seconds to process and there is about 5 seconds of processing time per second of time elapsed in the ultrasound image stack. The peak memory used for the given runtime is about 1.1 MB and the allocated memory is about 2.1 GB.

VI. Technical Discussion

The forward model we've created and the iterative inverse model in which we've nested the forward model have several assumptions previously mentioned which make the physiology for straightforward and the simulation computationally more simple. In hindsight some of these assumptions seem appropriate to make and some seem suboptimal, hence the contrast between the CV values of the diastolic pressure compared with those of the systolic pressure.

Concerning the forward model, the quadratic stress-strain relationship for tissue is a simplification of an Ogden hyperelastic model [11] and the linear stress-strain for the carotid vessel wall is also a simplification of a different hyperelastic model [15]. Moreover, the forward model presented is entirely lossless under all external forces (stresses) and uniformity assumptions on stiffness and pressure parameters are made throughout distinct regions. The pulsation force acting on the inside of the walls of the artery is also entirely assumed into the change in pressure. Finally, in order to most accurately portray the system, dimensionality of the model should be increased from one to three, given the physiology is realistically three-dimensional and the type of numerical model should be finite element instead of finite difference.

Concerning the iterative inverse model, the optimization method used is fast and perfectly stable for our given four parameters and our simplified one-dimensional system. However, there are other optimization methods that could scale better with number of parameters [16] [17] and be more robust to nonlinearity, multi-dimensionality, and ill-conditioned parameters [18]. Furthermore, a Kalman filter could be used to reduce the observational noise from the image segmentation and external force observation [19] [20].

VII. Ethics

Although this project has the goal of improving healthcare for cardiovascular disease by creating a numerical technique using FCU to provide clinical information, it still presents ethical issues and potential conflicts of interest with regard to its results reporting, publicizing, and clinical adoption.

Stakeholders consist of the inventors of the method, the doctors and hospitals who adopt the method, the patients who are assessed by the method, and all industry or even academic individuals responsible for the distribution, facilitation, and sales of the method. An ethically pure outcome for the method would be to help as many people as possible while harming nobody. However, this outcome will be difficult to attain given the method has significant technical merit. This reality is largely due to the stakeholders.

In the United States, healthcare is treated as a commodity. Therefore, it is often the case that if one wants to get an medical device or algorithm to positively impact lives, one will have to fundraise. Most often, investors would like to maximize their profits. Therefore a developer of this method may be coerced into deliberately increasing the procedural costs of the method which could cause the overall impact to be less positive. Additionally, in the acquiring of intellectual property, a developer of this method could be pressured into stretching the truth about the potential impact and accuracy of the method, possibly distracting from the feasible goals which one should strive towards. Finally, one can imagine a potential promoter of the method attempting to engage in a quip-pro-quo with its inventors with the goal of dishonestly advancing both parties' careers.

In order to effectively and ethically disclose and develop this method generalized to noninvasive vessel lumen pressure and wall stiffness determination, one must be aware of potential ethical pitfalls and take heed to avoid them.

VIII. Conclusions

We have demonstrated the use of one-dimensional forward numerical modeling in determining the displacement of nodes in a compression model of the human carotid artery. We have nested this forward model into an iterative inverse model where we optimize to determine the carotid artery lumen pressure wave as a function of time in addition to anterior tissue stiffness and carotid vessel wall stiffness quantification. Despite several simplifying assumptions, our numerical modeling provided a ballpark estimate of the entire carotid artery lumen pressure wave, something currently only able to be done clinically through invasive means. This progress is encouraging for future research.

REFERENCES

[1] Aaron Zakrzewski, Brian Anthony. "Noninvasive Blood Pressure Estimation Using Ultrasound and Simple Finite Element Models". IEEE Transactions on Biomedical Engineering. 2018.

[2] Robin Singh, Alex Jaffe, et al. "Noninvasive Assessment of Jugular Venous Pressure via Force-Coupled Single Crystal Ultrasound". *IEEE Transactions on Biomedical Engineering*. 2017.

[3] Chonghe Wang, et al. "Monitoring of the Central Blood Pressure Waveform Via a Conformal Ultrasonic Device". *Nature Biomedical Engineering*. 2018.

[4] "FastStats - Leading Causes of Death." *Centers for Disease Control and Prevention, Centers for Disease Control and Prevention*. 2017. www.cdc.gov/nchs/fastats/leading-causes-of-death.htm.

[5] Braunwald E. Heart Disease. 1988.

[6] Genest J, McPherson R, Frohlich J, Anderson T, Campbell N, Carpentier A, Couture P, Dufour R, Fodor G, Francis GA, Grover S. 2009 Canadian Cardiovascular Society/Canadian guidelines for the diagnosis and treatment of dyslipidemia and prevention of cardiovascular disease in the adult–2009 recommendations. Canadian Journal of Cardiology. 2009 Oct 1;25(10):567-79.

[7] Wong SN, Sung RY, Leung LC. "Validation of three oscillometric blood pressure devices against auscultatory mercury sphygmomanometer in children". *Blood Pressure Monitoring*. 2006.

[8] Heald CL, Fowkes FG, Murray GD, Price JF. "Ankle Brachial Index Collaboration. Risk of mortality and cardiovascular disease associated with the ankle-brachial index: systematic review". *Atherosclerosis*. 2006.

[9] Fung, Yuan-cheng. Biomechanics: mechanical properties of living tissues. Springer Science Business Media, 2013.

[10] N. Ozkaya et al. "Mechanical Properties of Biological Tissues". *Fundamentals of Biomechanics: Equilibrium, Motion, and Deformation.* 2012.

[11] Kevin M. Moerman, Ciaran K. Simms, Thomas Nagel. "Control of Tension–compression Asymmetry in Ogden Hyperelasticity with Application to Soft Tissue Modelling". *Journal of the Mechanical Behavior of Biomedical Materials*. 2015.

[12] Aaron Zakrzewski. "Arterial Blood Pressure Estimation Using Ultrasound." *MIT Mechanical Engineering*. 2017.

[13] Daniel, L 2019, Lecture 12 Nonlinear Steady State Analysis, lecture notes, Introduction to Numerical Simulation and Modeling 6.336, MIT, delivered 16 October 2019.

[14] Kim K, Weitzel WF, Rubin JM, Xie H, Chen X, O'Donnell M. "Vascular intramural strain imaging using arterial pressure equalization." *Ultrasound in medicine biology.* 2004.

[15] Balzani D, Deparis S, Fausten S, Forti D, Heinlein A, Klawonn A, Quarteroni A, Rheinbach O, Schröder J. "Numerical modeling of fluid–structure interaction in arteries with anisotropic polyconvex hyperelastic and anisotropic viscoelastic material models at finite strains." *International journal for numerical methods in biomedical engineering.* 2016.

[16] Cao, Yang, et al. "Adjoint sensitivity analysis for differential-algebraic equations: The adjoint DAE system and its numerical solution." *SIAM Journal on Scientific Computing*. 2003.

[17] Johnson, Steven G. "Notes on Adjoint Methods for 18.335." *Numerical Methods for Applied Mathematics*. 2012.

[18] Manolis IA Lourakis. "A brief description of the levenberg-marquardt algorithm implemented by levmar". *Foundation of Research and Technology*. 2005.

[19] Welch G, Bishop G. *An introduction to the Kalman filter.* 1995.

[20] Greenleaf JF, Kinnick R, Tan W, Chen S, Zheng Y. Detection of tissue harmonic motion induced by ultrasonic radiation force using pulse-echo ultrasound and Kalman filter. IEEE transactions on ultrasonics, ferroelectrics, and frequency control. 2007